AIAA JOURNAL
Vol. 44, No. 11, November 2006

Aeroelastic Damping Model Derived from Discrete Euler Equations

M. A. Woodgate* and K. J. Badcock†
University of Liverpool, Liverpool, L69 3BX England, United Kingdom

DOI: 10.2514/1.23637

The prediction of flutter onset based on aerodynamic modeling using computational fluid dynamics can be made using an augmented system of equations. Computational times similar to those required for computational fluid dynamics steady-state calculations have been reported for wing test cases. However, for such methods to be fully useful, information about damping must be obtainable without reverting to full-order time-domain simulation. This paper presents a method for computing damping based on a reduced-order modeling approach that systematically derives a two-degrees-of-freedom model from the full discrete system of equations. The method is based on a change of variables that employs the critical eigenvector of the aeroelastic system. The ability of this model to predict the damping for a model problem and for two wing test cases is shown.

Nomenclature

A	=	Jacobian matrix
E	=	fluid total energy
F	=	nonlinear part of $\boldsymbol{R}$
$\boldsymbol{F}, \boldsymbol{G}, \boldsymbol{H}$	=	convective flux vectors
$\boldsymbol{f}$	=	force acting at the grid points
h	=	grid spacing in the tubular reactor test problem
P	=	fluid pressure
Pe_h, Pe_m	=	constants in the tubular reactor test problem
$\boldsymbol{p}$	=	critical eigenvector of A^T, $p_1 + ip_2$
$\boldsymbol{q}$	=	critical eigenvector of A, $\boldsymbol{q}_1 + i\boldsymbol{q}_2$
$\boldsymbol{q}_s$	=	constant scaling vector
$\boldsymbol{R}$	=	residual function
$\mathbf{S}$	=	transformation function between aerodynamic and structural grids
t	=	real time
U, V, W	=	contravariant Cartesian fluid velocity components
u, v, w	=	Cartesian fluid velocity components
$\boldsymbol{w}$	=	state variables
x, y, z	=	Cartesian coordinates
$\boldsymbol{x}$	=	grid locations
$\mathbf{Y}$	=	unknown in the tubular reactor test problem
$\boldsymbol{y}$	=	part of $\boldsymbol{w}$ not in the critical space
$\mathbf{z}$	=	part of $\boldsymbol{w}$ in the critical space
α	=	structural modal coordinate
α_0	=	constant in the tubular reactor test problem
$\beta, \bar{\Theta}$	=	constants in the tubular reactor test problem
δ	=	change in grid locations
Θ	=	unknown in the tubular reactor test problem
μ	=	bifurcation parameter
ρ	=	fluid density
ϕ	=	structural mode shape
ψ_i^0	=	blending function for transfinite interpolation
ω	=	frequency of critical eigenvalue

Subscripts

A	=	of augmented system
a	=	aerodynamic
s	=	structural
0	=	values at the bifurcation point

Superscripts

i	=	inviscid
T	=	transpose

Presented as Paper 2021 at the 47th AIAA/ASME/ASCE/AHS/ASC Structures, Structural Dynamics, and Materials Conference, Newport, Rhode Island, 1–4 May 2006; received 4 March 2006; revision received 17 April 2006; accepted for publication 7 May 2006.

*Research Assistant, Computational Fluid Dynamics Laboratory, Flight Sciences and Technology, Department of Engineering.

†Professor, Computational Fluid Dynamics Laboratory, Flight Sciences and Technology, Department of Engineering; K.J.Badcock@liverpool.ac.uk.

Introduction

COMPUTATIONAL aeroelasticity has developed rapidly, with attention focusing on time-marching calculations using CFD, where the response of a system to an initial perturbation is calculated to determine growth or decay, and from this to infer stability. Recent and impressive example calculations have been made for complete aircraft configurations (see [1–3] amongst others).

The time-domain method is powerful because of its generality and ease of use. However, basing an investigation of system dynamics in the time domain has one major drawback, namely, the computational cost. This has led to an intensive effort to extract the useful information out of the full CFD model of the aerodynamics to provide a cheaper model that still retains the essential physics of the problem. Examples include proper orthogonal decomposition [4] (which involves the extraction of modes using a limited set of time snapshots of the flow evolution), a Volterra series (which relates the aerodynamic response to some input by a kernel [4]), and system identification (where a linear model is calculated from a limited time evolution of the aerodynamic response to some input). To date, no single method has proved its utility on general aeroelastic problems.

Arguably the most advanced reduced-order method is proper orthogonal decomposition (POD). A set of solutions (steady and unsteady) are generated for prescribed conditions and motions. For example, in [5] the POD modes are calculated for the AGARD wing based on forced motions in the frequency range of interest for the structural modes. From this information, a small-order model was developed and the behavior of the aeroelastic eigenspectrum, which could be calculated for the reduced system, was examined. This approach was used to compute limit-cycle behavior for an airfoil [6], and access to the complete eigenspectrum provided good insights into the physical behavior.

However, it is clear from the literature (for example [4,5,7]) that the phenomena which are relevant for a particular problem must be present in the training solutions for the modes. Aspects such as the mean shock location and the range of shock motion must be well covered. In this respect, the problems examined in the literature are

not representative of general three-dimensional problems with strong aerodynamic nonlinearities. First, the AGARD wing has a small number of important modes and no strong shock at any Mach number. Secondly, the two-dimensional airfoil problems have a limited number of modes of motion. Thirdly, the problems currently tackled are normally symmetric, which leads to the important simplification that the steady state is independent of the dynamic pressure. Fourthly, the need to generate snapshots using multiple time-domain calculations provides a computational overhead before the reduced model is generated. It is therefore clear that POD is a powerful method that is meeting with some success. However, for the reasons listed, the approach is not currently a general purpose tool for investigating aeroelastic problems (strong shocks, multiple modes of structural motion, and asymmetric geometry) at low cost.

Motivated by these factors, an alternative approach is being investigated. Recent work has built on the ideas first presented by Morton and Beran in [8] to calculate the onset of flutter through a Hopf Bifurcation of the full CFD/FEM system. This is achieved through the solution of a modified system of equations at a cost comparable to a steady-state CFD solution, giving a considerable advantage compared with using unsteady calculations to bracket the flutter speed. Successful application of the method was made for airfoils in [9] and for wings in [10]. Because the approach is based on the full system residual and its Jacobian matrix, which encapsulates the physics of the problem directly through conservation laws, it has the potential to deal with general aerodynamic nonlinearities. In addition, the cost of the approach can potentially be driven down to that of a conventional steady-state calculation (which is significantly less than the training time required for POD). To realize this potential, results have to be obtained for asymmetric problems in viscous flow, and work is ongoing toward this end.

Although knowledge of the onset of instability is important, other pieces of information are required in practice. For example, flight tests measure damping and compare this with predictions to inform decisions about future test points. If the stability boundary is to be crossed in flight, then knowledge of the limit-cycle oscillation amplitude is required. If this requires recourse to time-domain simulations, then much of the advantage of the methods of the previous paragraph is lost. A systematic approach to model reduction is therefore required to supplement the rapid prediction of the flutter point.

The perturbation method of multiple scales can be applied to determine behavior close to a bifurcation. This approach was used in [11] for a two-dimensional aeroelastic problem and was presented in [12] for the Duffing oscillator and in [13] for a three-equation model problem. The idea is use a perturbation parameter ϵ to separate events at different time scales. The terms of $\mathcal{O}(\epsilon)$ provide a description of the linear dynamics of the system, and higher-order terms provide information about the effect of nonlinearities.

The center manifold theory provides a route to reducing a large dimension model to its essential dynamics. However, the practical obstacles to applying this approach to full-order systems of more than 10 degrees of freedom have proved formidable. The current paper addresses this problem by using a change of coordinates for the system variables that allows the reduced model to be derived while preserving most of the structure of the original system, making manipulation of the reduction practical. Information from the direct solution of the bifurcation point and its associated eigenvalue and eigenvectors [9,10] is used in this change of variables and the subsequent manipulation.

The current paper adopts this approach to calculating a reduced-order model. Further simplification of the approach is made for the prediction of damping, and the method is assessed for a model problem followed by application to two flexible wings. The full center manifold reduction is described in the Appendix. The full reduction relies on the calculation of the second and third Jacobian matrices of the discrete operator. For the tubular reactor model problem, these have been calculated analytically (helped by the relatively simple spatial finite differences used in this case). For the aeroelastic systems, matrix-free products (essentially finite differences) are required to calculate these terms. These calculations have not been implemented in the current paper. The paper continues with the formulation of the reduced modeling, followed by a description of the full-order systems. Results are then presented and evaluated, followed by conclusions.

Formulation

Stability Calculation

Consider the nonlinear system of equations

$$\dot{\boldsymbol{w}} = \boldsymbol{R}(\boldsymbol{w}, \mu), \qquad \boldsymbol{w} \in \Re^n \tag{1}$$

An equilibrium $\boldsymbol{R}(\boldsymbol{w}_0, \mu) = 0$ experiences a loss of stability through a Hopf bifurcation for values of μ such that $\partial \boldsymbol{R}/\partial \boldsymbol{w} = A(\mathbf{w}_0, \mu)$ has a pair of eigenvalues $\pm i\omega$ that cross the imaginary axis. Denoting the corresponding eigenvector by $\boldsymbol{q} = \boldsymbol{q}_1 + i\boldsymbol{q}_2$, the behavior of the critical eigenpair ω and $\boldsymbol{q}$ can be written as

$$A\boldsymbol{q} = i\omega\boldsymbol{q} \tag{2}$$

This equation can be written in terms of real and imaginary parts as $A\boldsymbol{q}_1 + \omega\boldsymbol{q}_2 = 0$ and $A\boldsymbol{q}_2 - \omega\boldsymbol{q}_1 = 0$. A unique eigenvector is chosen by scaling against a constant real vector $\boldsymbol{q}_s$ to produce a chosen complex value, taken to be $0 + 1i$. This yields two additional scalar equations $\boldsymbol{q}_s^T\boldsymbol{q}_1 = 0$ and $\boldsymbol{q}_s^T\boldsymbol{q}_2 - 1 = 0$.

A bifurcation point can be calculated directly by solving the augmented system of equations:

$$\boldsymbol{R}_A(\boldsymbol{w}_A) = 0 \tag{3}$$

where

$$\boldsymbol{R}_A = \begin{bmatrix} \boldsymbol{R} \\ A\boldsymbol{q}_1 + \omega\boldsymbol{q}_2 \\ A\boldsymbol{q}_2 - \omega\boldsymbol{q}_1 \\ \boldsymbol{q}_s^T\boldsymbol{q}_1 \\ \boldsymbol{q}_s^T\boldsymbol{q}_2 - 1 \end{bmatrix} \tag{4}$$

and $\boldsymbol{w}_A = [\boldsymbol{w}, \boldsymbol{q}_1, \boldsymbol{q}_2, \mu, \omega]^T$.

The bifurcation point can be calculated through a solution of Eq. (4) using Newton's method. This has been achieved for airfoils free to move in pitch and plunge [9] and for flexible wings [10]. Full details of the calculation method are given in those references.

Damping Calculation

The eigenvector that goes critical at a Hopf bifurcation will also be the least lightly damped mode for parameter values in a region below the bifurcation value. In this region, the asymptotic damping value will be determined by this mode. It is possible to reduce the full system by a change of variables to calculate the damping by only considering a low dimension reduced model. For aeroelastic systems, we are dealing with systems of large dimension, and it is advantageous to use a change of variable that involves manipulating the system in its original form as far as possible. A summary of the general formulation based on the center manifold theory is given in the Appendix. In this section, a simpler version of the general theory is given to allow damping to be calculated.

The full system can be transformed by using only the vectors corresponding to the critical eigenvalues of A and its transpose A^T. These are calculated from Eq. (4). The system is projected onto its critical eigenspace and complement. Suppose we have a Taylor expansion of the residual function $\boldsymbol{R}$ about the equilibrium solution $\boldsymbol{w}_0$ and parameter at the bifurcation point μ_0, giving

$$\dot{\bar{\boldsymbol{w}}} = A\bar{\boldsymbol{w}} + F(\bar{\boldsymbol{w}}, \bar{\mu}), \qquad \boldsymbol{w} \in \Re^n \tag{5}$$

where $F(\bar{\boldsymbol{w}}, \bar{\mu})$ has at least quadratic terms and $\bar{\boldsymbol{w}} = \boldsymbol{w} - \mathbf{w}_0$, $\bar{\mu} = \mu - \mu_0$. The matrix A has a pair of complex eigenvalues on the imaginary axis $\lambda_{1,2} = i\omega$, $\omega > 0$. Let $\boldsymbol{q}$ be the right eigenvector corresponding to λ_1. Then $\bar{\boldsymbol{q}}$ is the right eigenvector corresponding to λ_2 and

$$A\boldsymbol{q} = i\omega\boldsymbol{q}, \qquad A\bar{\boldsymbol{q}} = -i\omega\bar{\boldsymbol{q}}$$

The left eigenvector $\boldsymbol{p}$ has the same property

$$A^T\boldsymbol{p} = -i\omega\boldsymbol{p}, \qquad A^T\bar{\boldsymbol{p}} = i\omega\bar{\boldsymbol{p}}$$

These can be normalized such that $\langle \boldsymbol{p}, \boldsymbol{q}\rangle = 1$, where $\langle \boldsymbol{p}, \boldsymbol{q}\rangle = \sum_{i=1}^{n} \bar{\boldsymbol{p}}_i \boldsymbol{q}_i$. The eigenspace S corresponding to $\pm i\omega$ is two-dimensional and is spanned by $\{\Re\boldsymbol{q}, \Im\boldsymbol{q}\}$. The eigenspace T corresponds to all the other eigenvalues of A and is $(n-2)$ dimensional. Then $\boldsymbol{y} \in T$ if, and only if, $\langle \boldsymbol{q}, \boldsymbol{y}\rangle = 0$. Because $\boldsymbol{y} \in \Re^n$ whereas $\boldsymbol{p}$ is complex, then two real constraints on $\boldsymbol{y}$ exist and hence it is possible to decompose any $\bar{\boldsymbol{w}} \in \Re^n$ as

$$\bar{\boldsymbol{w}} = \mathbf{z}\boldsymbol{q} + \bar{\mathbf{z}}\,\bar{\boldsymbol{q}} + \boldsymbol{y}$$

where $\mathbf{z} \in C^1$, $\mathbf{z}\boldsymbol{q} + \bar{\mathbf{z}}\,\bar{\boldsymbol{q}} \in S$, and $\boldsymbol{y} \in T$. The complex variable $\mathbf{z}$ is a coordinate of S and so

$$\begin{cases} \mathbf{z} = \langle \boldsymbol{p}, \bar{\mathbf{w}}\rangle \\ \boldsymbol{y} = \bar{\boldsymbol{w}} - \langle \boldsymbol{p}, \bar{\boldsymbol{w}}\rangle\boldsymbol{q} - \langle \bar{\boldsymbol{p}}, \bar{\boldsymbol{w}}\rangle\bar{\boldsymbol{q}} \end{cases}$$

because $\langle \boldsymbol{p}, \bar{\boldsymbol{q}}\rangle = 0$. The Eq. (5) then has the form

$$\begin{cases} \dot{\mathbf{z}} = i\omega\mathbf{z} + \langle \boldsymbol{p}, F(\mathbf{z}\boldsymbol{q} + \bar{\mathbf{z}}\,\bar{\boldsymbol{q}} + \boldsymbol{y}, \bar{\mu})\rangle \\ \dot{\boldsymbol{y}} = A\boldsymbol{y} + F(\mathbf{z}\boldsymbol{q} + \bar{\mathbf{z}}\,\bar{\boldsymbol{q}} + \boldsymbol{y}, \bar{\mu}) - \langle \boldsymbol{p}, F(\mathbf{z}\boldsymbol{q} + \bar{\mathbf{z}}\,\bar{\boldsymbol{q}} + \boldsymbol{y}, \bar{\mu})\rangle\boldsymbol{q} - \langle \boldsymbol{p}, F(\mathbf{z}\boldsymbol{q} + \bar{\mathbf{z}}\,\bar{\boldsymbol{q}} + \boldsymbol{y}, \bar{\mu})\rangle\bar{\boldsymbol{q}} \end{cases}$$

This system is $(n+2)$ dimensional but we have two constraints on $\boldsymbol{y}$.

Now, in general at this stage, a center manifold reduction should be used to obtain a relationship between $\boldsymbol{y}$ and $\mathbf{z}$ that allows the critical dynamics to be calculated from the $\mathbf{z}$ equation only. This treatment allows nonlinear features such as limit-cycle oscillations to be calculated from the reduced model. A description of the method to perform this reduction is given in the Appendix and is referred to in the results section as the *center manifold reduced model*. Here we are interested in calculating damping for parameter values below the bifurcation point. In this case, the influence of the component $\boldsymbol{y}$ from the noncritical space is damped faster than the critical component $\mathbf{z}$. We therefore neglect the influence of $\boldsymbol{y}$ altogether, which removes the need for the center manifold reduction. Further justification for this approximation will be given in the results section.

The damping is therefore determined by solving the equation

$$\dot{\mathbf{z}} = i\omega\mathbf{z} + \langle \boldsymbol{p}, F(\mathbf{z}\boldsymbol{q} + \bar{\mathbf{z}}\,\bar{\boldsymbol{q}}, \bar{\mu})\rangle$$

This system is two-dimensional. Finally, we need to calculate the form of F. Expanding the function $\boldsymbol{R}$ in a Taylor series about the equilibrium solution $\boldsymbol{w}_0$ and parameter μ_0 gives

$$\begin{aligned} \boldsymbol{R}(\bar{\boldsymbol{w}}, \bar{\mu}) = \boldsymbol{R}(\boldsymbol{w}_0, \mu_0) &+ \frac{\partial \boldsymbol{R}}{\partial \boldsymbol{w}}\bar{\boldsymbol{w}} \\ &+ \frac{1}{2}\frac{\partial^2 \boldsymbol{R}}{\partial \boldsymbol{w}^2}\bar{\boldsymbol{w}}\,\bar{\boldsymbol{w}} + \frac{1}{6}\frac{\partial^3 \boldsymbol{R}}{\partial \boldsymbol{w}^3}\bar{\boldsymbol{w}}\,\bar{\boldsymbol{w}}\,\bar{\boldsymbol{w}} + \frac{\partial \boldsymbol{R}}{\partial \mu}\bar{\mu} + \frac{1}{2}\frac{\partial^2 \boldsymbol{R}}{\partial \mu^2}\bar{\mu}^2 + \frac{1}{6}\frac{\partial^3 \boldsymbol{R}}{\partial \mu^3}\bar{\mu}^3 \\ &+ \frac{\partial^2 \boldsymbol{R}}{\partial \mu \partial \boldsymbol{w}}\bar{\mu}\,\bar{\boldsymbol{w}} + \frac{1}{2}\frac{\partial^3 \boldsymbol{R}}{\partial \mu^2 \partial \boldsymbol{w}}\bar{\mu}^2\bar{\boldsymbol{w}} + \frac{1}{2}\frac{\partial^3 \boldsymbol{R}}{\partial \mu \partial \boldsymbol{w}^2}\bar{\mu}\,\bar{\boldsymbol{w}}\,\bar{\boldsymbol{w}} + \cdots \end{aligned}$$

where all derivatives are evaluated at $(\boldsymbol{w}_0, \mu_0)$. We can simplify this by noting that $\boldsymbol{R}(\boldsymbol{w}_0, \mu_0) = 0$ and neglecting terms that are quadratic and higher in $\bar{\boldsymbol{w}}$ and $\bar{\mu}$. This leaves

$$\boldsymbol{R}(\bar{\boldsymbol{w}}, \bar{\mu}) \approx A\bar{\boldsymbol{w}} + \frac{\partial \boldsymbol{R}}{\partial \mu}\bar{\mu} + \frac{\partial A}{\partial \mu}\bar{\mu}\,\bar{\boldsymbol{w}}$$

which means that

$$F(\bar{\boldsymbol{w}}, \bar{\mu}) = \boldsymbol{R}_\mu\bar{\mu} + A_\mu\bar{\mu}\,\bar{\boldsymbol{w}} \tag{6}$$

and hence

$$\langle \boldsymbol{p}, F(\mathbf{z}\boldsymbol{q} + \bar{\mathbf{z}}\,\bar{\boldsymbol{q}}, \bar{\mu})\rangle = \langle \boldsymbol{p}, \boldsymbol{R}_\mu\bar{\mu}\rangle + \langle \boldsymbol{p}, A_\mu\bar{\mu}\,\bar{\boldsymbol{w}}\rangle$$

Using the change of coordinates and pulling the values of $\mathbf{z}$ and $\bar{\mathbf{z}}$ through the inner product, we obtain

$$\langle \boldsymbol{p}, \bar{\mu}A_\mu\bar{\boldsymbol{w}}\rangle = \mathbf{z}\langle \boldsymbol{p}, \bar{\mu}A_\mu\boldsymbol{q}\rangle + \bar{\mathbf{z}}\langle \boldsymbol{p}, \bar{\mu}A_\mu\bar{\boldsymbol{q}}\rangle$$

This allows the reduced model to be written as a constant coefficient two-degrees-of-freedom system.

This model is referred to in the results section as the *damping reduced model*. If the term F is neglected altogether, then we only retain linear terms, and this is referred to as the *linear reduced model*. Further simplification of the damping reduced model is possible for the aeroelastic system and will be discussed next.

To summarize, the damping calculation proceeds in the following steps:

1) Using the direct solver, calculate the Hopf bifurcation point, the critical eigenvalue, and the corresponding eigenvector of A^T.

2) Calculate the projected two-degrees-of-freedom model using

$$\dot{\mathbf{z}} = i\omega\mathbf{z} + \mathbf{z}\langle \boldsymbol{p}, \bar{\mu}A_\mu\boldsymbol{q}\rangle + \bar{\mathbf{z}}\langle \boldsymbol{p}, \bar{\mu}A_\mu\bar{\boldsymbol{q}}\rangle$$

3) Use the two-degrees-of-freedom model to compute the response of $\mathbf{z}$ to an initial disturbance for values of $\mu < \mu_0$. This solution can be transformed back to the original variables using

$$\bar{\boldsymbol{w}} = \mathbf{z}\boldsymbol{q} + \bar{\mathbf{z}}\,\bar{\boldsymbol{q}}$$

Two-Dimensional Nonadiabatic Tubular Reactor with Axial Mixing

To test the solution methodology for the augmented system, a model problem is considered that describes the unsteady behavior of a nonadiabatic tubular reactor with axial mixing [14,15]:

$$\begin{aligned} \frac{\partial Y}{\partial t} &= \frac{1}{Pe_m}\frac{\partial^2 Y}{\partial x^2} - \frac{\partial Y}{\partial x} - \mu Y \exp\left(\Gamma - \frac{\Gamma}{\Theta}\right) \\ \frac{\partial \Theta}{\partial t} &= \frac{1}{Pe_h}\frac{\partial^2 \Theta}{\partial x^2} - \frac{\partial \Theta}{\partial x} - \beta(\Theta - \bar{\Theta}) + \mu\alpha_0 Y \exp\left(\Gamma - \frac{\Gamma}{\Theta}\right) \end{aligned} \tag{7}$$

where Pe_m, Pe_h, β, α_0, Γ, and $\bar{\Theta}$ are fixed constants, and μ is the bifurcation parameter. The boundary conditions ($t > 0$) are given by

$$\frac{\partial Y}{\partial x} = Pe_m(Y - 1), \qquad \frac{\partial \Theta}{\partial x} = Pe_m(\Theta - 1), \qquad (x = 0)$$

$$\frac{\partial Y}{\partial x} = \frac{\partial \Theta}{\partial x} = 0 \qquad (x = 1)$$

For the results presented here, the constants are set to $Pe_m = 5$, $Pe_h = 5$, $\beta = 2.5$, $\alpha_0 = 0.5$, $\Gamma = 25$, and $\bar{\Theta} = 1.0$.

The system is discretized using a cell-centered finite difference scheme so that the first and second differences are approximated by

$$\left.\frac{\partial^2 Y}{\partial x^2}\right|_i = \frac{Y_{i+1} - 2Y_i + Y_{i-1}}{h^2}, \qquad \left.\frac{\partial Y}{\partial x}\right|_i = \frac{Y_{i+1} - Y_{i-1}}{2h}$$

Here a uniform mesh of spacing h is used with the ith point at $x_i = ih$ for $(i = 0, \ldots, n)$. The boundary conditions for $x = 1$ are applied by

setting halo cell values to be identical to the values in the adjacent interior cell.

The solution for an equilibrium and also of the augmented system is by the full Newton method with the use of the exact Jacobian on the left-hand side. For the augmented system and the various types of reduced model, the first- and second-order Jacobian terms have been calculated analytically and were checked using finite differences. To check the reduced results, unsteady time stepping is also considered. An explicit method is used that results in a large number of time steps ($\Delta t = 1/500$ is required for stability). The bifurcation point is bracketed between a steady solution at one parameter value and an unsteady solution at a second value. Each new calculation halves the length of the region bracketing the bifurcation value.

3-D Aeroelastic System Based on the Euler Equations

The three-dimensional Euler equations can be written in conservative form and Cartesian coordinates as

$$\frac{\partial \boldsymbol{w}_f}{\partial t} + \frac{\partial \mathbf{F}^i}{\partial x} + \frac{\partial \mathbf{G}^i}{\partial y} + \frac{\partial \mathbf{H}^i}{\partial z} = 0 \tag{8}$$

where $\boldsymbol{w}_f = (\rho, \rho u, \rho v, \rho w, \rho E)^T$ denotes the vector of conserved variables. The flux vectors $\boldsymbol{F}^i$, $\boldsymbol{G}^i$ and $\boldsymbol{H}^i$ are

$$\boldsymbol{F}^i = \begin{pmatrix} \rho U^* \\ \rho u U^* + P \\ \rho v U^* \\ \rho w U^* \\ U^*(\rho E + P) + \dot{x} \end{pmatrix} \tag{9}$$

$$\boldsymbol{G}^i = \begin{pmatrix} \rho V^* \\ \rho u V^* \\ \rho v V^* + P \\ \rho w V^* \\ V^*(\rho E + P) + \dot{y} \end{pmatrix} \qquad \boldsymbol{H}^i = \begin{pmatrix} \rho \boldsymbol{W}^* \\ \rho u \boldsymbol{W}^* \\ \rho v \boldsymbol{W}^* + P \\ \rho w \boldsymbol{W}^* + P \\ \boldsymbol{W}^*(\rho E + P) + \dot{z} \end{pmatrix} \tag{10}$$

where U^*, V^*, and $\boldsymbol{W}^*$ are the three Cartesian components of the velocity relative to the moving coordinate system, which has local velocity components $\dot{x}$, $\dot{y}$ and $\dot{z}$, that is,

$$U^* = u - \dot{x} \tag{11}$$

$$V^* = v - \dot{y} \tag{12}$$

$$\boldsymbol{W}^* = w - \dot{z} \tag{13}$$

The wing deflections $\delta \boldsymbol{x}_s$ are defined at a set of points $\boldsymbol{x}_s$ by

$$\delta \boldsymbol{x}_s = \Sigma \alpha_i \phi_i \tag{14}$$

where ϕ_i are the mode shapes calculated from a full finite element model of the structure and α_i are the generalized coordinates. By projecting the finite element equations onto the mode shapes, the scalar equations

$$\frac{\mathrm{d}\alpha_i}{\mathrm{d}t^2} + \omega_i^2 \alpha_i = \mu \phi_i^T \boldsymbol{f}_s \tag{15}$$

are obtained where $\boldsymbol{f}_s$ is the vector of aerodynamic forces at the structural grid points, and $\mu = c^5 \rho_\infty U_\infty^2$. These equations are rewritten as a system in the form

$$\frac{\mathrm{d}\boldsymbol{w}_s}{\mathrm{d}t} = \boldsymbol{R}_s \tag{16}$$

where $\boldsymbol{w}_s = (\ldots, \alpha_i, \dot{\alpha}_i, \ldots)^T$ and $\boldsymbol{R}_s = (\ldots, \dot{\alpha}_i, \mu \phi_i^T \boldsymbol{f}_s - \omega_i^2 \alpha_i, \ldots)^T$.

The aerodynamic forces are calculated at face centers on the aerodynamic surface grid and these must be transferred to the structural grid. This problem was considered in [16,17], where a method was developed called the constant volume tetrahedron (CVT) transformation. Denoting the fluid grid locations and aerodynamic forces as $\boldsymbol{x}_a$ and $\boldsymbol{f}_a$, then

$$\delta \boldsymbol{x}_a = \mathcal{S}(\boldsymbol{x}_a, \boldsymbol{x}_s, \delta \boldsymbol{x}_s)$$

where $\mathcal{S}$ denotes the relationship defined by CVT. In practice, this equation is linearized to give

$$\delta \boldsymbol{x}_a = S(\boldsymbol{x}_a, \boldsymbol{x}_s) \delta \boldsymbol{x}_s$$

and then by the principle of virtual work, $\boldsymbol{f}_s = S^T \boldsymbol{f}_a$.

The grid speeds on the wing surface are also needed and these are approximated directly from the linearized transformation as

$$\delta \dot{\boldsymbol{x}}_a = S(\boldsymbol{x}_a, \boldsymbol{x}_s) \delta \dot{\boldsymbol{x}}_s$$

where the structural grid speeds are given by

$$\delta \dot{\boldsymbol{x}}_s = \Sigma \dot{\alpha}_i \phi_i \tag{17}$$

We have to deal with the deforming geometry. This is achieved using transfinite interpolation (TFI) of displacements within the blocks containing the wing. The wing surface deflections are interpolated to the volume grid points $\boldsymbol{x}_{ijk}$ as

$$\delta \boldsymbol{x}_{ijk} = \psi_j^0 \delta \boldsymbol{x}_{a,ik} \tag{18}$$

where ψ_j^0 are values of a blending function [18] that varies between one at the wing surface (here $j = 1$) and zero at the block face opposite. The surface deflections $\boldsymbol{x}_{a,ik}$ are obtained from the transformation of the deflections on the structural grid and so ultimately depend on the values of α_i. The grid speeds can be obtained by differentiating Eq. (18) to obtain their explicit dependence on the values of $\dot{\alpha}_i$.

We will consider the bifurcation parameter as μ. For symmetric wings at zero incidence, any equilibrium solution has the wing undeflected. This means that $\boldsymbol{f}_s = 0$ at the equilibrium solution. The fluid equations do not depend explicitly on μ. Therefore $\boldsymbol{f}_\mu = 0$ in Eq. (4) for an equilibrium solution. Also, the linear dependence of the structural equations on μ means that A_μ is constant and only has nonzero terms in the small number of rows corresponding to the structural equations.

Results

Tubular Reactor

The rich solution space for this model problem is shown in Fig. 1. This includes stable and unstable equilibria, limit points, and Hopf bifurcation points. There is also a hysteresis loop for increasing and decreasing μ. The solution is characterized by the maximum value of Θ within the domain. The equilibrium solutions for varying μ are shown in Fig. 1. For $\mu < 0.165$ and $\mu > 0.180$, this equilibrium is

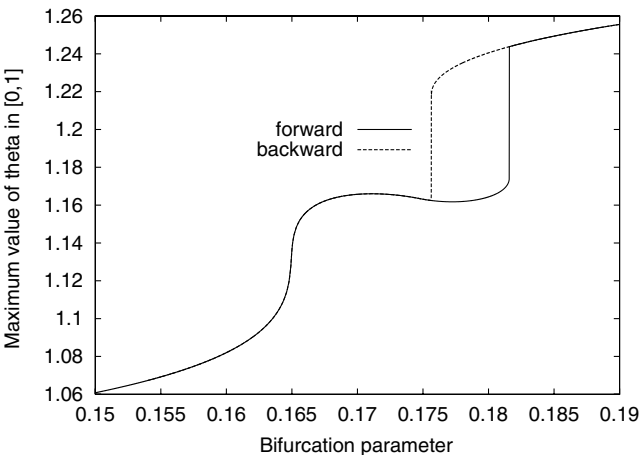

Fig. 1 The equilibrium solution as mapped out by a continuation method, varying the bifurcation parameter μ.

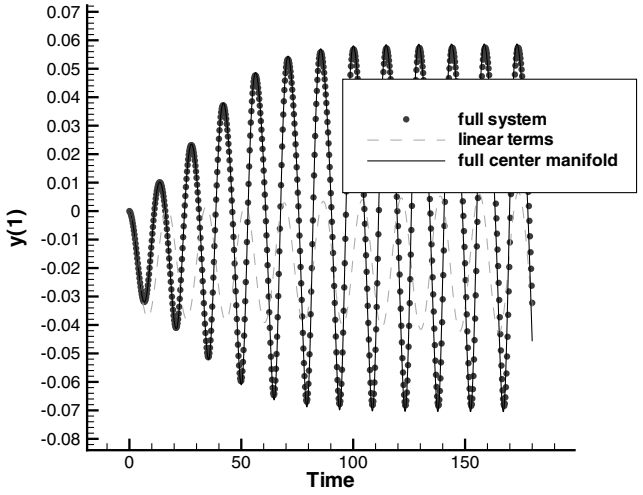

Fig. 2 Comparison of results for an LCO response at $\bar{\mu} = 0.00007$.

stable and the solution to Eq. (7) is steady. For $0.165 < \mu < 0.180$, the equilibrium is unstable and a limit-cycle oscillation is formed. Depending on whether the parameter μ is increased (solid line) or decreased (solid switching to dashed lines with increasing μ), a different equilibrium is obtained, indicating hysteresis. The equilibria were mapped out using a continuation method with Newton's method for the corrector stage. In addition, time-marching calculations were done to map out the stability of these equilibria.

Next, the augmented system [Eq. (3)] was solved to find the bifurcation points. If the initial guess is poor, then the solution diverges. For the current calculations, the following initial guess was used: $\mu = 0.16$, $x_{2i} = 1.0$, $x_{2i+1} = 0.0$, $P_{1_i} = \sqrt{n1}$, $P_{2_{2i}} = \sqrt{n1}$, $P_{2_{2i+1}} = -\sqrt{n1}$, $\boldsymbol{q} = P_2$, and the eigenvalue i. By changing the initial conditions, the Newton iterations can be made to converge to the second Hopf point at $\mu = 0.180$. Starting from this guess, the iterations had to be underrelaxed by a factor 0.5 until the domain of quadratic convergence was reached (the criteria used were based on the initial residual being reduced by half). A sequence of grids was used to show mesh independence, and a second method of initialization was used by taking the final solution from the previous grid in the sequence as the starting solution on the next grid. No relaxation was required using this technique.

Damping calculations were made using the reduced model. Various results are compared to gain some insight into the behavior of the different options. The benchmark is the time-domain solution of the full system, which is indicated by the dots on the time response curves. Secondly, the full center manifold reduction is based on the Taylor expansion of the residual, including third-order terms, and using the reduction methodology described in the Appendix. Finally, the key results are obtained using the simpler damping reduction using the Taylor expansion of Eq. (6).

We consider results about the bifurcation point $\mu_0 = 0.16508$ and for values of $\bar{\mu}$ of -0.00005, -0.0001, and -0.0002. Although it is beyond the scope of this paper, results are also shown in Fig. 2 for $\bar{\mu} = 0.00007$, which results in a limit cycle. The center manifold reduction predicts the limit cycle oscillation (LCO) response perfectly.

The damped responses for $\bar{\mu} = -0.00005$, $\bar{\mu} = -0.0001$, and $\bar{\mu} = -0.0002$ are shown in Fig. 3. The center manifold results, which arise from solving a two-degrees-of-freedom system, agree perfectly with the full-order (here, 512 degrees of freedom) system results for all three cases. Finally, the damping reduced model predicts the response very well. Given the relative simplicity of calculating the damping reduced model, these results suggest a strong preference for this approach.

AGARD 445.6 Wing

The behavior of the method is next investigated for the aeroelastic response of the AGARD 445.6 wing. Time-domain and bifurcation results are given in [10]. The grid has 17,900 points and is optimized to have a large number of points in the tip region, which is critical for

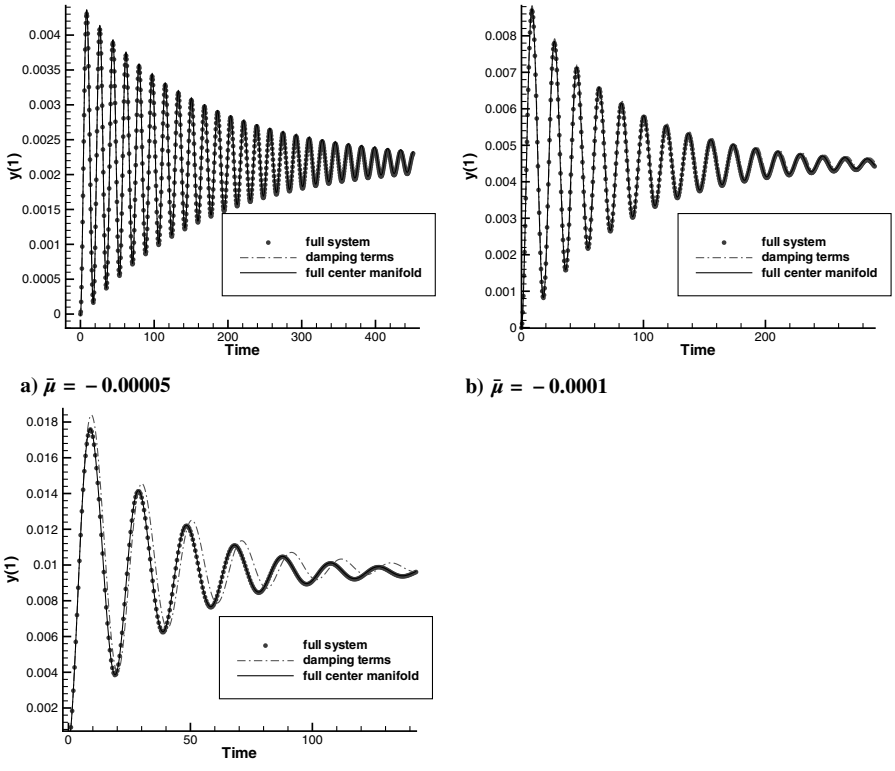

a) $\bar{\mu} = -0.00005$ **b) $\bar{\mu} = -0.0001$**

c) $\bar{\mu} = -0.0002$

Fig. 3 Comparison of results for damped responses at $\bar{\mu} = -0.00005$, $\bar{\mu} = -0.0001$, and $\bar{\mu} = -0.0002$.

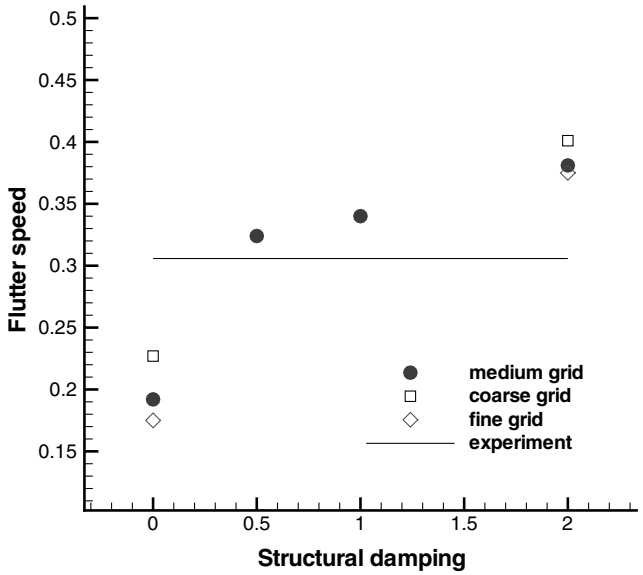

Fig. 4 The variation of flutter speed index with the structural damping applied at Mach 0.96. The line indicates the measurement. Reproduced from [10].

predicting flutter onset. The four important modes from the structural model, which is of the plate variety, were retained.

In a previous paper [10], a detailed evaluation of the stability boundary calculation is given. Two factors were found to be important, namely, grid refinement and the influence of structural damping. Calculations on grids with up to 1.4 million points were made, with grid convergence trends obtained. The effect of grid refinement was to decrease the flutter speed index. Interestingly, in the bottom of the dip, the fine grid Euler solution is significantly below the measured value (and is in fact further from the measurement than the coarse grid solutions). By adding a small amount of structural damping, the grid converged value can be shifted back onto the measured value. These results are summarized in Fig. 4, which is reproduced from [10]. The grid used in the current study is slightly coarser than the coarse grid referred to in the figure and gives a very similar stability boundary.

The aeroelastic root loci at a freestream Mach number of 0.97 have been traced out using the inverse power method. This calculation is based on the full discrete system matrices, with the initial shift chosen to be the structural frequency. These are shown in Fig. 5 and show the

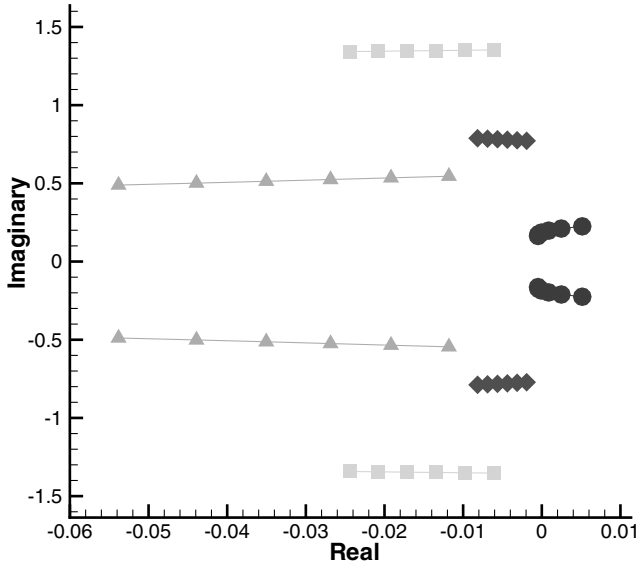

Fig. 5 Aeroelastic root loci at Mach 0.97, traced by the inverse power method working on the full discrete system.

first structural mode crossing the imaginary axis. It is interesting to compare this plot with the one shown in [5], which was derived from the reduced system based on POD modes.

Next, the reduced damping model predictions were calculated for values of dynamic pressure, which are 5, 10, 20, and 40% below the bifurcation value for Mach numbers of 0.67, 0.90, 0.96, and 1.07. The reduced model (two degrees of freedom) responses are compared with the full-order system (89,508 degrees of freedom) in Figs. 6–9. A number of comments can be made. First, as the dynamic pressure tends to the flutter value, the reduced model predictions converge to those of the full model as expected. The more heavily damped results at $M = 0.67$ show more discrepancy than the other three cases, which show good agreement, even at 60% of the flutter value. It is possible that the addition of higher-order terms from the center manifold reduction may allow improved prediction for the heavily damped cases and this will be investigated in future work. The typical CPU time for a full-order time-domain calculation is 142 times that of a steady-state calculation. The reduced model takes a negligible time to run, and is formed (once only for each Mach number) at a cost comparable to 3.2 steady-state calculations. Once formed, the responses can be approximated almost free for any value of the dynamic pressure below the critical value.

Hawk Wing

Finally, we present results representing the wing of the Hawk trainer, which is manufactured by BAE Systems. A previous study of the flutter characteristics of this aircraft was reported in [3] using the time-domain approach. Predictions for several models of the Hawk were compared, including a linear method, a CFD-based model of the wing–body–tailplane, and the wing alone.

In the current calculations, an aerodynamic grid with 16,644 points was generated, which was found to give reliable results in the previous paper through a grid refinement study. The structural dynamics are represented by a beam model, supplied by BAE Systems. A full description of how the transformation is done from this structural model is given in [3]. The four lowest frequency symmetric nontailplane modes in the structural model are retained for the flutter calculations. These have frequencies of 12.42 Hz (first wing bending), 14.43 Hz (the influence of the first fuselage bending mode on the wing), 32.46 Hz (the influence of the second fuselage bending mode on the wing), and 37.87 Hz (the first wing torsion mode). In the linear aeroelastic predictions made with the same four modes, the first wing bending and torsion modes couple, the other two modes having only a small influence on the flutter mechanism. This structural model provided an ideal test case for the CFD-based methods. The full aerostructural model has 16,652 degrees of freedom.

The bifurcation solver was first used to trace out the flutter boundary which is shown in Fig. 10. The prediction of damping was then evaluated for the Mach number, which results in the lowest point on the transonic flutter dip. Values of dynamic pressure at 98, 95, and 92% of the critical value were chosen. Even at 98% of the critical value, the damping is heavy, in contrast with the AGARD wing for the Mach number in the flutter dip.

The comparison between the damping reduced model and the full-order model is shown in Fig. 11. The agreement at 98% of the critical value is close and, in terms of damping, the reduced-model predictions are not too dissimilar at 95 and 92%, either. However, close inspection of the comparisons shows that the frequencies of the responses at the lower two values are significantly in disagreement. Calculation of the eigenspectrum by the inverse power method shows that the closest mode to the imaginary axis is the critical mode only after the bifurcation parameter is 96% of the critical value. Below this, a lower frequency mode dominates the response.

The time-domain calculation of the full-order system in this cases took in excess of 10 h on a Pentium 4 processor. The reduced model took less than 20 s to compute the same case.

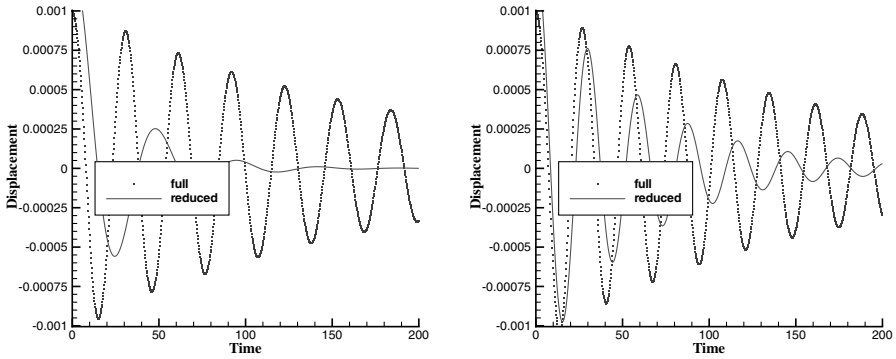

a) 60% b) 80%

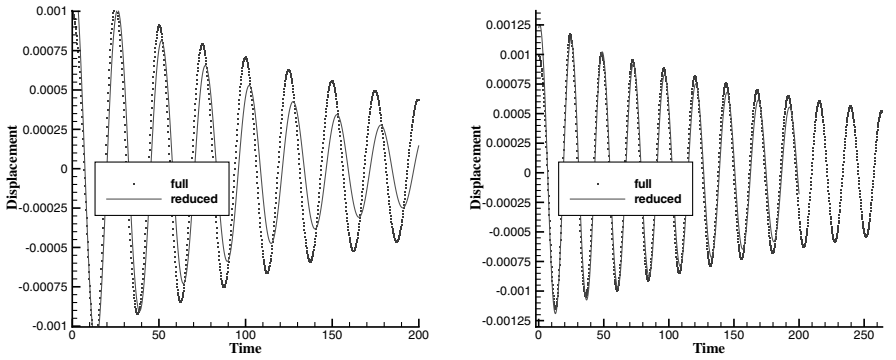

c) 90% d) 95%

Fig. 6 Comparison of results from the full model and damping reduced model at $M = 0.67$ for values of dynamic pressure below the flutter boundary.

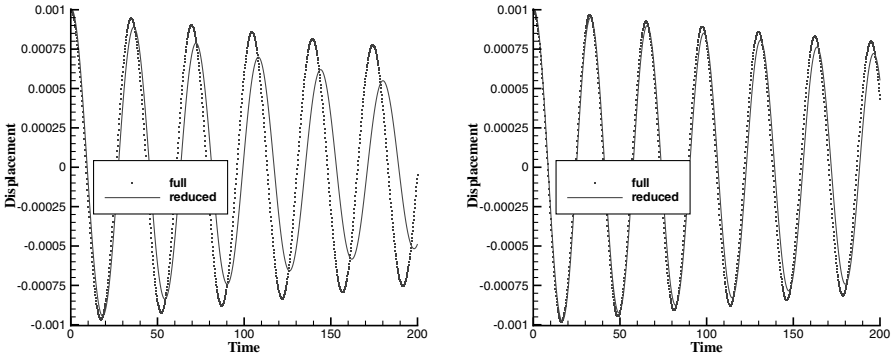

a) 60% b) 80%

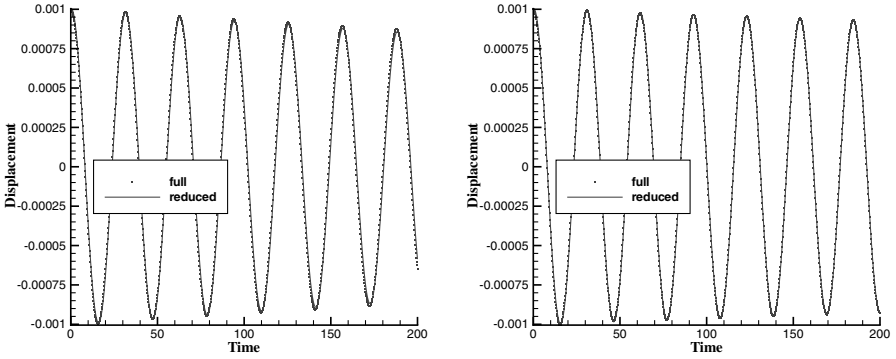

c) 90% d) 95%

Fig. 7 Comparison of results from the full model and damping reduced model at $M = 0.90$ for values of dynamic pressure below the flutter boundary.

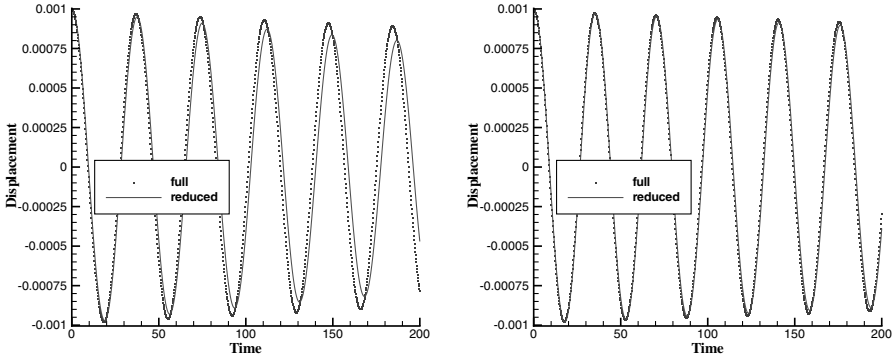

a) 60% b) 80%

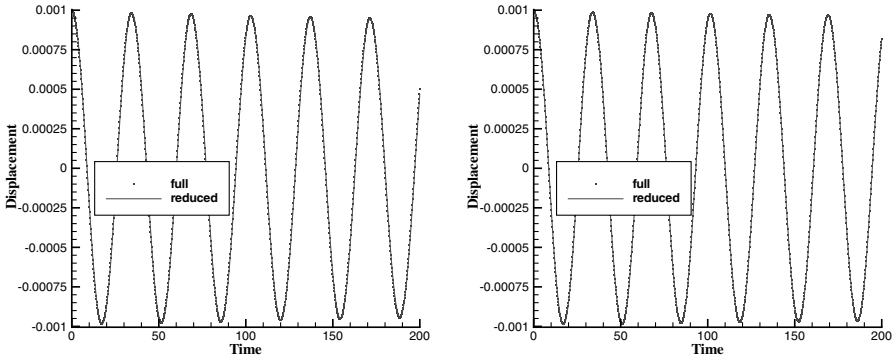

c) 90% d) 95%

Fig. 8 Comparison of results from the full model and damping reduced model at $M = 0.96$ for values of dynamic pressure below the flutter boundary.

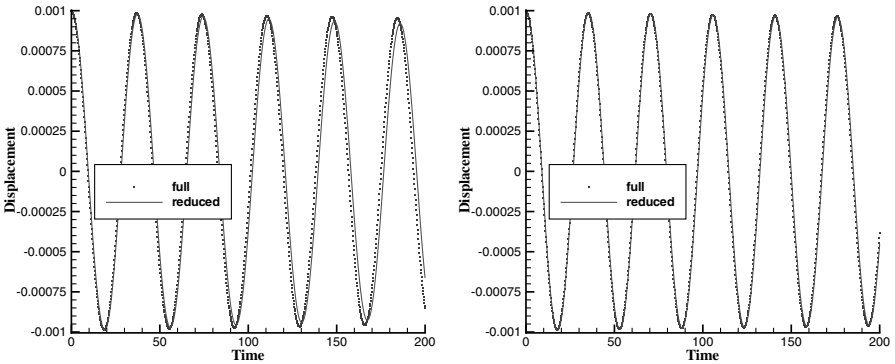

a) 60% b) 80%

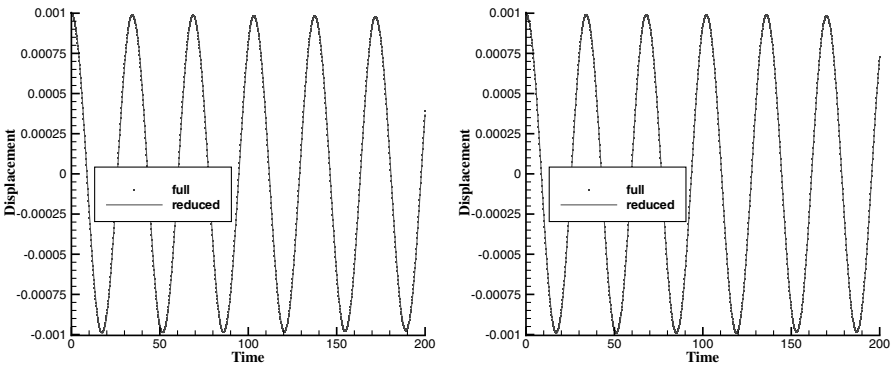

c) 90% d) 95%

Fig. 9 Comparison of results from the full model and damping reduced model at $M = 1.07$ for values of dynamic pressure below the flutter boundary.

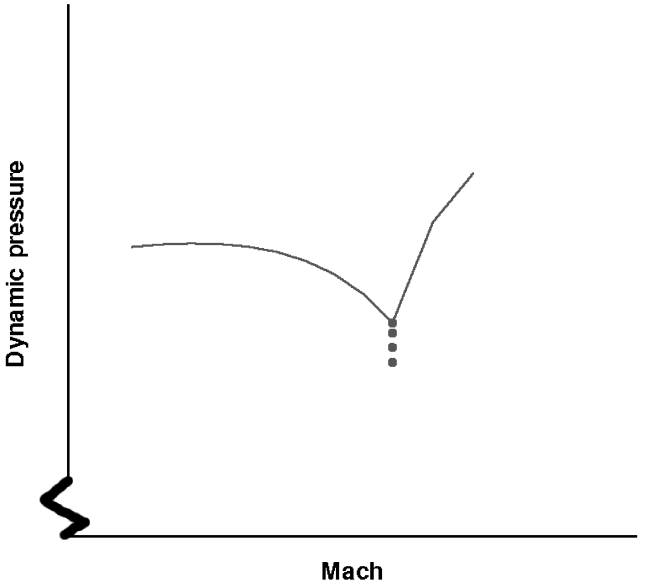

Fig. 10 Flutter boundary for Hawk wing traced out using the bifurcation solver. The values of dynamic pressure at which the damping model is compared with full-order results are indicated by the dots.

Conclusion

Previous work has shown that the flutter onset speed can be computed for CFD–CSD coupled models using fast methods based on the behavior of the critical eigenvalue. Flutter speeds can be computed in roughly the cost of a steady-state calculation, avoiding the large costs associated with time-domain analysis.

In the current paper, a method that uses information available about the critical eigenvector of the system has been presented that forms a two-degrees-of-freedom model to compute the damped response at values of the dynamic pressure below the critical value. This information has the potential to allow rapid evaluation of damping characteristics before flight testing.

Results were shown for a tubular reactor model problem and then for the aeroelastic behavior of the AGARD and Hawk wings. Close to the critical parameter value, the full-order system response is reproduced well by the two-degrees-of-freedom model. As the response becomes more heavily damped, the agreement becomes less good, but these cases are also less critical in the real situation.

Results using a center manifold correction were presented for the tubular reactor model problem and excellent agreement was obtained with the full-order system, even for heavily damped conditions.

Further work is required to make the approach generally applicable. First, a parallel implementation of the calculations is required to allow large systems to be tackled. Secondly, viscous terms need to be included in the stability calculation. Thirdly, second and third Jacobian vector products are required for the full center manifold calculation of aeroelastic systems. This would open up the potential for calculating limit-cycle responses via the reduced model.

Appendix: Classical Model Reduction

Consider the nonlinear system of equations

$$\dot{x} = \boldsymbol{f}(x), \qquad x \in \Re^n \tag{A1}$$

where $\boldsymbol{f}$ is sufficiently smooth. We assume that we are at a Hopf bifurcation and hence the Jacobian matrix $\partial \boldsymbol{f}/\partial x$ has two, and only two, critical eigenvalues with zero real part and the remaining $m = n - 2$ eigenvalues have negative real parts. Then the system in Eq. (A1) can be transformed to

$$\begin{cases} \dot{u} = Bu + g(u, v) \\ \dot{v} = Cv + h(u, v) \end{cases} \tag{A2}$$

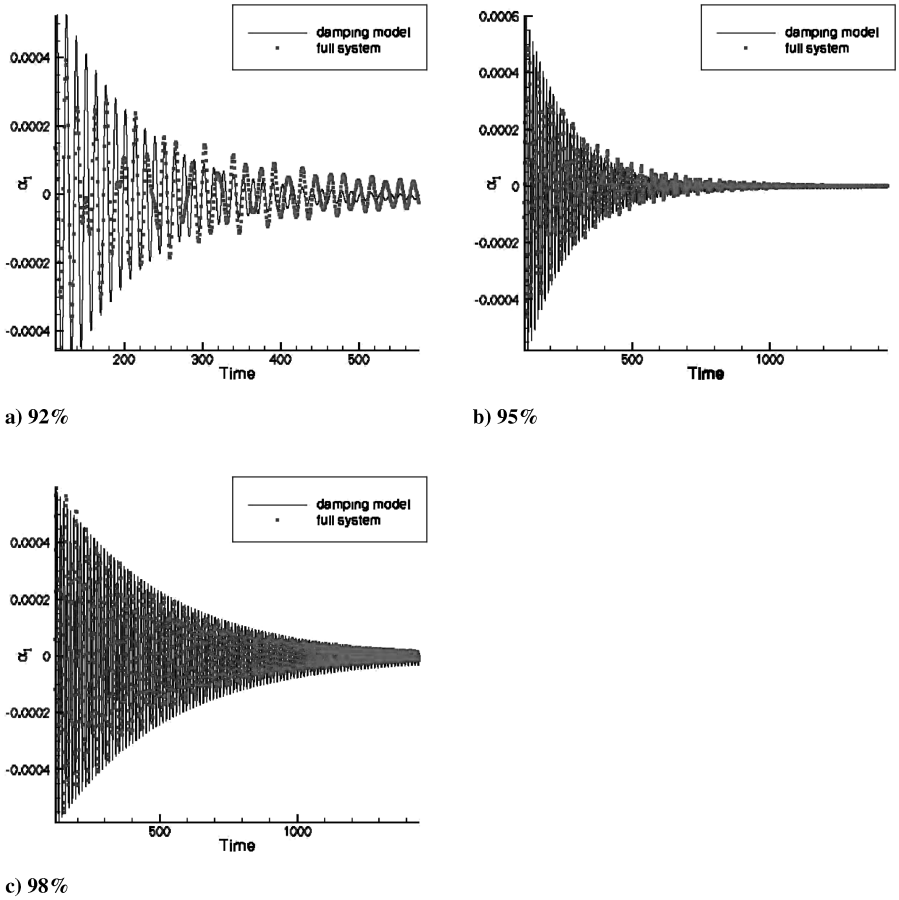

Fig. 11 Comparison of results for the Hawk wing in the transonic dip for values of dynamic pressure below the flutter boundary.

where $u \in \Re^2$ and $v \in \Re^m$. B is a 2×2 matrix with its eigenvalues on the imaginary axis and C is an $m \times m$ matrix with no eigenvalues on the imaginary axis. The functions g and h have at least quadratic terms. The center manifold $\boldsymbol{W}^c$ of the system in Eq. (A2) can be locally represented as a graph of a smooth function,

$$\boldsymbol{W}^c = \{(u, v): v = V(u)\} \tag{A3}$$

V: $\Re^2 \to \Re^m$ and due to the tangent property of $\boldsymbol{W}^c$, $V(u) = \mathcal{O}(\|u\|^2)$.

The reduction principle says the system in Eq. (A2) is locally topologically equivalent near the origin to

$$\begin{cases} \dot{u} = Bu + g(u, V(u)) \\ \dot{v} = Cv \end{cases} \tag{A4}$$

The important thing to notice is that the equations for u and v are decoupled in Eq. (A4). The first equation is the restriction of the system in Eq. (A2) to its center manifold. The dynamics of the structurally unstable system in Eq. (A2) are essentially determined by this restriction, because the second equation in Eq. (A4) is linear. For a Hopf bifurcation with ($\lambda_{1,2} = \pm i\omega$), then, the system looks like

$$\begin{cases} \begin{pmatrix} \dot{u}_1 \\ \dot{u}_2 \end{pmatrix} = \begin{pmatrix} 0 & -\omega \\ \omega & 0 \end{pmatrix} \begin{pmatrix} u_1 \\ u_2 \end{pmatrix} + \begin{pmatrix} G_1(u_1, u_2, v) \\ G_2(u_1, u_2, v) \end{pmatrix} \\ \dot{v} = Cv + H_1(u_1, u_2, v) \end{cases} \tag{A5}$$

It is possible to rewrite this in complex form by use of the variable $z = u_1 + iu_2$ to obtain

$$\begin{cases} \dot{z} = i\omega z + G(z, \bar{z}, v) \\ \dot{v} = Cv + H(z, \bar{z}, v) \end{cases} \tag{A6}$$

where G and H are smooth complex-valued functions of z, and $\bar{z} \in C^1$ of at least quadratic order. The center manifold $\boldsymbol{W}^c$ can be locally represented as a graph of a smooth function:

$$\boldsymbol{W}^c = \{(z, v): v = V(z)\}$$

V maps $\Re^2 \to \Re^{n-2}$ and due to the tangent property of $\boldsymbol{W}^c$, $V(z) = \mathcal{O}\|u\|^2$. The center manifold $\boldsymbol{W}^c$ therefore has the representation

$$v = V(z, \bar{z}) = \tfrac{1}{2} w_{20} z^2 + w_{11} z\bar{z} + \tfrac{1}{2} w_{02} \bar{z}^2 + \mathcal{O}(|z|^3) \tag{A7}$$

with the coefficients $w_{ij} \in C^2$. Because v must be real, w_{11} is real and $w_{20} = \bar{w}_{02}$. Using Taylor expansions in z, $\bar{z}$, and v, the system in Eq. (A6) can be rewritten as

$$\begin{cases} \dot{z} = i\omega z + \tfrac{1}{2} G_{20} z^2 + G_{11} z\bar{z} + \tfrac{1}{2} G_{02} \bar{z}^2 + \tfrac{1}{2} G_{21} z^2 \bar{z} + \langle G_{10}, v \rangle z + \langle G_{01}, v \rangle \bar{z} + \cdots \\ \dot{v} = Cv + \tfrac{1}{2} H_{20} z^2 + H_{11} z\bar{z} + \tfrac{1}{2} H_{02} \bar{z}^2 + \cdots \end{cases} \tag{A8}$$

where G_{20}, G_{11}, G_{02}, and $G_{21} \in C^1$ and G_{01}, G_{10}, and $H_{ij} \in C^{n-2}$. Because v is real, H_{11} is real, and $H_{20} = \bar{H}_{02}$.

$$G_{jk} = \frac{\partial^{j+k}}{\partial z^j \partial \bar{z}^k} G(z, \bar{z}, 0)\bigg|_{z=0}, \qquad j + k \geq 2 \tag{A9}$$

$$\bar{G}_{10,j} = \frac{\partial^2}{\partial v_j \partial z} G(z, \bar{z}, v)\bigg|_{z=0, v=0}, \qquad j = 1, 2, \ldots, n-2 \tag{A10}$$

$$\bar{G}_{01,j} = \frac{\partial^2}{\partial v_j \partial \bar{z}} G(z, \bar{z}, v)\bigg|_{z=0, v=0}, \qquad j = 1, 2, \ldots, n-2 \tag{A11}$$

$$H_{jk} = \frac{\partial^{j+k}}{\partial z^j \partial \bar{z}^k} H(z, \bar{z}, 0)\bigg|_{z=0}, \qquad j + k = 2 \tag{A12}$$

On substituting the representation of the center manifold in Eq. (A8) and equating coefficients,

$$\begin{aligned} &w_{20} = (2i\omega I - C)^{-1} H_{20}, \qquad w_{11} = -C^{-1} H_{11}, \\ &w_{02} = (-2i\omega I - C)^{-1} H_{20} \end{aligned} \tag{A13}$$

Where I is the identity matrix and the matrices $(2i\omega I - C)$, C, and $(-2i\omega I - C)$ are invertible because 0 and $\pm 2i\omega$ are not eigenvalues of C.

For reduction to be worthwhile, the bifurcation parameter must also be added to the system and included in the calculated center manifolds. This allows the reduced model to be applied for parameter values away from the bifurcation value. Consider the parameterized equation

$$\dot{x} = F(x, \alpha)$$

where $x \in \Re^n$ and $\alpha \in \Re^m$. Suppose that at $\alpha = 0$ the system has a nonhyperbolic equilibrium $x = 0$ that undergoes a Hopf bifurcation. This means we have a system equivalent to

$$\begin{cases} \dot{u} = Bu + g(u, v, \alpha) \\ \dot{v} = Cv + h(u, v, \alpha) \end{cases} \tag{A14}$$

and because α does not depend on time, we can append the equation $\dot{\alpha} = 0$ to the expanded system:

$$\begin{cases} \dot{u} = Bu + g(u, v, \alpha) \\ \dot{v} = Cv + h(u, v, \alpha) \\ \dot{\alpha} = 0 \end{cases} \tag{A15}$$

The center manifold theorem asserts the existence of a center manifold for the origin that is local, given by points (u, v, α) satisfying an equation of the form

$$v = k(u, \alpha)$$

This is used in the reduction step.

Acknowledgements

This work was supported by BAE Systems, the Engineering and Physical Sciences Research Council, and the Ministry of Defence, and is part of the work program of the Partnership for Unsteady Methods in Aerodynamics (PUMA) Defence and Aerospace Research Partnership (DARP).

References

[1] Farhat, C., Geuzaine, P., and Brown, G., "Application of a Three-Field Nonlinear Fluid-Structure Formulation to the Prediction of The Aeroelastic Parameters of an F-16 Fighter," *Computers and Fluids*, Vol. 32, No. 1, Jan. 2003, pp. 3–29.

[2] Melville, R., "Nonlinear Simulation of F-16 Aeroelastic Instability," AIAA Paper 2001-0570, 2001.

[3] Woodgate, M. A., Badcock, K. J., Rampurawala, A. M., Richards, B. E., Nardini, D., and Henshaw, M., "Aeroelastic Calculations for the Hawk Aircraft Using the Euler Equations," *Journal of Aircraft*, Vol. 42, No. 4, 2005, pp. 1005-1012.

[4] Lucia, D. J., Beran, P. S., and Silva, W. A., "Reduced-Order Modeling: New Approaches for Computational Physics," *Progress in Aerospace Sciences*, Vol. 40, No. 1–2, 2004, pp. 51–117.

[5] Thomas, J. P., Dowell, E. H., and Hall, K. C., "Three-Dimensional Transonic Aeroelasticity Using Proper Orthogonal Decomposition-Based Reduced-Order Models," *Journal of Aircraft*, Vol. 40, No. 3, 2003, pp. 544-551.

[6] Dowell, E. H., Thomas, J. P., and Hall, K. C., "Transonic Limit Cycle Oscillation Analysis Using Reduced Order Aerodynamic Models," *Journal of Fluids and Structures*, Vol. 19, No. 1, 2004, pp. 17–27.

[7] Badcock, K. J., Allan, M. R., and Beran, P. S., "Fast Prediction of Wing Rock Onset Based on Computational Fluid Dynamics," *Confederation of European Aerospace Societies/AIAA/Deutsche Gesellschaft für Luft- und Raumfarht International Forum for Aeroelasticity and Structural Dynamics*, CEAS/AIAA/DGLR Paper IF-072, 2005.

[8] Morton, S. A., and Beran, P. S., "Hopf-Bifurcation Analysis of Airfoil Flutter at Transonic Speeds," *Journal of Aircraft*, Vol. 36, No. 2, 1999, pp. 421–429.

[9] Badcock, K. J., Woodgate, M. A., and Richards, B. E., "The Application of Sparse Matrix Techniques for the CFD Based Aeroelastic Bifurcation Analysis of a Symmetric Aerofoil," *AIAA Journal*, Vol. 42, No. 5, May 2004, pp. 883–892.

[10] Badcock, K. J., Woodgate, M. A., and Richards, B. E., "Direct Aeroelastic Bifurcation Analysis of a Symmetric Wing Based on the Euler Equations," *Journal of Aircraft*, Vol. 42, No. 3, 2005, pp. 731–737.

[11] Beran, P. S., "Computation of a Limit-Cycle Oscillation Using a Direct Method," AIAA Paper 1999-1462, 1999.

[12] Nayfeh, A. H., and Balachandran, B., *Applied Nonlinear Dynamics*, Wiley, New York, 1995.

[13] Nayfeh, A. H., and Balachandran, B., "Motion Near a Hopf Bifurcation of a Three-Dimensional System," *Mechanics Research Communications*, Vol. 17, No. 4, 1990, pp 191–198.

[14] Ortiz, E. L., "Step by Step Tau Method Part 1: Piecewise Polynomial Approximations," *Computers and Mathematics with Applications*, Vol. 1, Nos. 3–4, 1975, pp. 381–392.

[15] Beran, P. S., and Carlson, C. D., "Domain-Decomposition Methods for Bifurcation Analysis," AIAA Paper 97-0518, 1997.

[16] Goura, G. S. L., "Time Marching Analysis of Flutter Using Computational Fluid Dynamics," Ph.D. Thesis, Univ. of Glasgow, Glasgow, Scotland, U.K., Nov. 2001.

[17] Goura, G. S. L., Badcock, K. J., Woodgate, M. A., and Richards, B. E., "Extrapolation Effects on Coupled CFD-CSD Simulations," *AIAA Journal*, Vol 41, No. 2, 2003, pp. 312–314.

[18] Gordon, W. J., and Hall, C. A., "Construction of Curvilinear Coordinate Systems and Applications to Mesh Generation," *International Journal for Numerical Methods in Engineering*, Vol. 7, No. 4, 1973, pp. 461–477.

E. Livne
Associate Editor